A Mechanistic Rationale for the Mode Selectivity in the Intramolecular Cyclization of Ethylene-Tethered Iminoketenimines: [2+2] versus [4+2] Stepwise Cycloadditions

Mateo Alajarín,*[a] Pilar Sánchez-Andrada,*[a] Angel Vidal,[a] and Fulgencio Tovar[a]

Keywords: Ab initio and density functional calculations / Cumulenes / Cycloaddition / Reaction mechanisms / Schiff bases

A stepwise mechanism, via a zwitterionic intermediate, has been established by ab initio and DFT calculations for the intramolecular cyclization of *N*-(3-azabut-3-enyl)ketenimine into its corresponding [2+2] cycloadduct. The control of the mode selectivity ([2+2] versus [4+2] cycloaddition) in the intramolecular cyclization of *C*-vinyl-*N*-(iminoethylene)ketenimines, which favors the [4+2] cycloadducts, also has been rationalized by comparing the energies calculated for both reaction pathways; the results have been confirmed by a quantitative kinetic analysis.

Introduction

Probably the most versatile chemical behavior of ketenimines is their participation in formal pericyclic processes, such as [2+2] and [4+2] cycloadditions, electrocyclic ring closures, and sigmatropic rearrangements.[1−6] Amongst these reactions, the [2+2] and [4+2] cycloaddition processes have attracted the most attention.

Ketenimines undergo [2+2] cycloaddition, mainly involving their cumulative C=C double bond, with compounds containing carbon−heteroatom [C=X; e.g., imines, aldehydes, and (thio)ketones] or heteroatom−heteroatom (X=X; e.g., azo and nitroso compounds) double bonds.[3] The *intermolecular* version of the [2+2] cycloaddition of ketenimines with the C=N bond of imines was first reported by Regitz in 1979[7] and studied one year later by Ghosez;[8] both groups concluded that only the introduction of electron-withdrawing substituents on the nitrogen atom of the ketenimine, which enhances the electrophilic character of the heterocumulene, allows the cycloaddition to occur. Since then, these reaction remained unexplored until we reported recently the *intramolecular* [2+2] cycloaddition between ketenimines and imines supported on an allylic or *ortho*-benzylic scaffold,[9−14] which allows the constraints imposed to the *intermolecular* variant by the electronic nature of the substituents to be overcome.

On the other hand, ketenimines play different roles in [4+2] cycloadditions.[3] First, they can serve as the two-atom component, with either the C=N or C=C bond of the ketenimine being involved in the cycloaddition process. Secondly, ketenimines may act as the four-atom component, either reacting across the dienic system formed by their C=N bond and a conjugated C=C bond from a substituent on the nitrogen atom [*N*-vinyl(aryl) ketenimines], or reacting as an all-carbon diene using their cumulative C=C bond and a conjugated C=C bond on the sp^2-hybridized carbon atom terminus [*C*-vinyl(aryl) ketenimines]. Amongst all the reported examples of [4+2] cycloadditions of ketenimines, only a few deal with ketenimines acting as all-carbon dienes and imines as dienophiles.[15−18]

Our experimental findings on the study of the intramolecular cyclization of different types of iminoketenimines point out that the length and nature of the tether linking both functional groups — imine and ketenimine — are crucial in determining the chemical evolution of this class of heterocumulenes.[19] Recently, we studied the reactivity of iminoketenimines **1** bearing an ethylene tether, which is more flexible than the rigid or semi-rigid tethers utilized in previous experiments.[18] Iminoketenimines **1** were transformed into the oxidized [4+2] cycloadducts **2** by heating in toluene under reflux; the formation of the corresponding [2+2] cycloadducts **3** was not observed (Scheme 1).

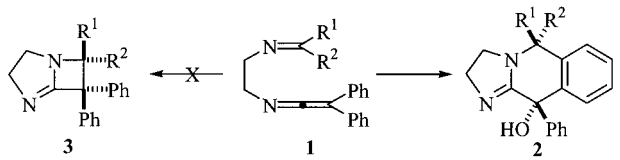

3 1 2

Scheme 1

Herein we disclose the results of a computational study undertaken with the aim of explaining these latter exper-

[a] Departamento de Química Orgánica, Facultad de Química, Universidad de Murcia,
Campus de Espinardo, 30100, Murcia, Spain
Fax: (internat.) +34-968-364149
E-mail: alajarin@um.es
Supporting information for this article is available on the WWW under http://www.eurjoc.org or from the author.

  DOI: 10.1002/ejoc.200400093

imental results, i.e., the control of the mode selectivity ([2+2] versus [4+2] cycloaddition) found in the cyclizations of the ethylene-tethered iminoketenimines **1**, which lead to **2** but not to **3**. We will show that this study offers a rational explanation of the experimental results. To the best of our knowledge, no computational studies on the competing [2+2] and [4+2] cycloadditions of imines with ketenimines have been published to date.[20]

Computational Details

The calculations were performed using the GAUSSIAN 98 suite of programs.[21] Geometry optimizations were carried out at the RHF, Becke3LYP,[22−25] and MP2[26−30] theoretical levels with the internal 6−31G* basis set.[31] All the reported stationary points were fully optimized by analytical gradient techniques. Harmonic frequency calculations at each level of theory verified the identity of each stationary point as a minimum or a transition state, and were used to provide an estimation of the zero-point vibrational energies (ZPVEs). The ZPVEs obtained at the HF/6-31G* and MP2/6-31G* levels were scaled by 0.8929 and 0.9646, respectively.[32] The ZPVEs obtained at the B3LYP/6-31G* level were not scaled. Atomic charges were calculated with the natural bond orbital method.[33−35]

Results and Discussion

First we explored the potential energy surface associated with the [2+2] intramolecular cycloaddition of the structurally most simple iminoketenimine bearing an ethylene tether connecting both nitrogen atoms, i.e., the transformation **4** → **5** (Scheme 2), with the dual aims of analyzing whether the [2+2] cycloaddition occurs by the same two-step mechanism established for related reactions and of finding an explanation for the apparent reluctance of this type of iminoketenimine to experience [2+2] cycloadditions. The chief geometrical features of the stationary points are reported in Figure 1. The qualitative reaction profile of this transformation is shown in Figure 2. With the aim of simplifying the discussion, we will comment only on the results obtained at the B3LYP/6-31G* theoretical level.

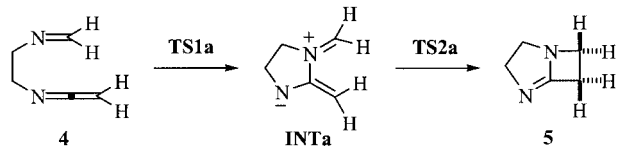

Scheme 2

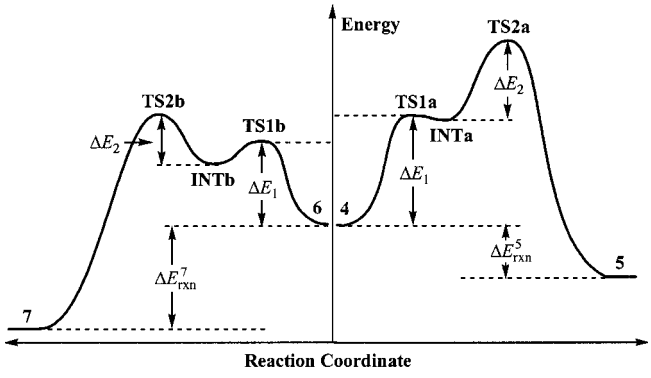

Figure 2. Qualitative reaction profile of the intramolecular [2+2] cycloaddition of **4** and **6** to yield the cycloadducts **5** and **7**, respectively, at the B3LYP/6-31G* theoretical level

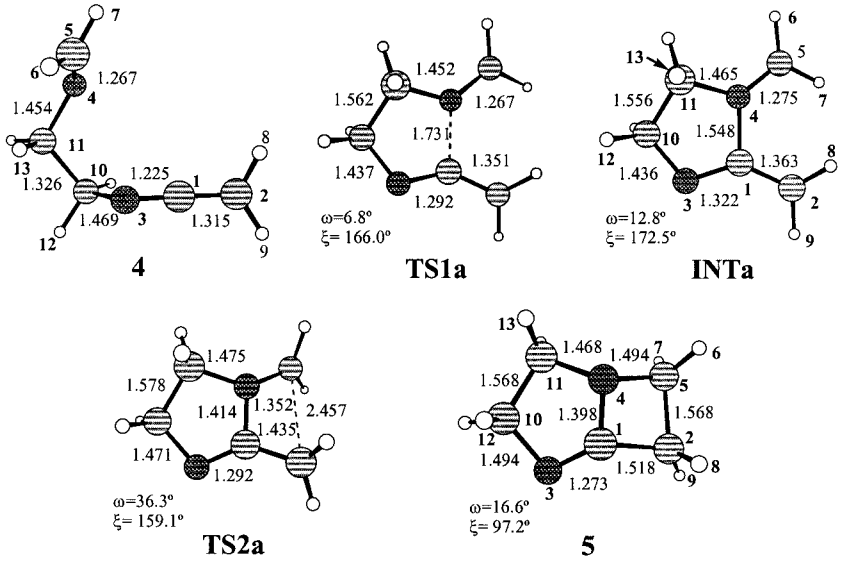

Figure 1. Computer plot of the stationary points found in the intramolecular [2+2] cycloaddition of **4** to yield **5**; plain numbers correspond to the geometrical parameters computed at the B3LYP/6-31G* level

The transformation **4** → **5** takes place by the same two-step mechanism described for other [2+2] cycloadditions of iminoketenimines,[11] which involves the formation of a zwitterionic intermediate. The first step consists of the nucleophilic attack of the iminic nitrogen atom on the sp-hybridized carbon atom of the ketenimine, through **TS1a**, and, thus, leading to **INTa**. In the second step, the 4π conrotatory ring closure of **INTa** occurs through **TS2a** to give the final bicyclic amidine **5**. All attempts to find a concerted pathway were unsuccessful.

The computed energy barriers are listed in Table 1, where, for comparative purposes, we have also included those corresponding to the previously computed intramolecular [2+2] cycloaddition of *N*-(4-azapenta-1,4-dienyl)ketenimine (**6**), which yields the azeto[2,1-*b*]pyrimidine **7** via the dipolar intermediate **INTb**, and the corresponding transition structures **TS1b** and **TS2b** (Scheme 3).[11]

Table 1. Energy barriers (ΔE, kcal mol^{-1}) computed for the transformations **4** → **5** and **6** → **7**

Method	ΔE_1[a]	ΔE_2	ΔE_{rxn}
4 → **5**			
HF/6-31G*[b]	35.75	28.19	−10.97
B3LYP/6-31G*[c]	24.40	16.90	−10.91
MP2/6-31G*[d]	24.06	16.16	−17.82
6 → **7**			
HF/6-31G*[b]	32.18	20.00	−24.38
B3LYP/6-31G*[c]	19.73	11.06	−22.57
MP2/6-31G*[b]	18.25	7.44	−30.34

[a] See Figure 2 for the notation of the energy barriers. [b] Energies computed on fully optimized HF/6-31G* geometries. The ZPVE corrections computed at the same level and appropriately scaled have been included. [c] Energies computed on fully optimized B3LYP/6-31G* geometries. The ZPVE corrections computed at the same level have been included. [d] Energies computed on fully optimized MP2/6-31G* geometries. The ZPVE corrections computed at the same level and appropriately scaled have been included.

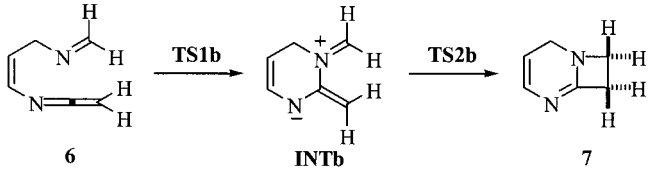

Scheme 3

First of all, the data presented in Table 1 reveal increases in the energy barriers associated with both the first and second steps of the transformation **4** → **5** when compared with those of **6** → **7**. This situation can be explained on electronic and geometrical grounds. The electrophilic character of the heterocumulenic moiety in ketenimine **6** is greater than that in **4** because of the presence of the C=C bond linked to the ketenimine nitrogen atom, which allows a certain degree of enamine-like resonance (Scheme 4).[11] Consequently, this effect decreases the first reaction barrier in **6** → **7** in relation to that in **4** → **5**, where the aliphatic tether connecting the nitrogen atoms lacks this type of electronic delocalization.

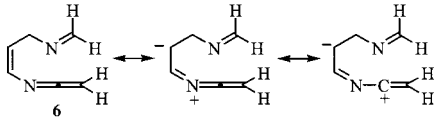

Scheme 4

With regard to the second step, several concurrent effects may be argued to explain why **TS2b** is earlier than **TS2a**. As far as the geometry of these transitions states is concerned, the ω torsional angle between the two terminal interacting carbon atoms (as defined in Figure 3) is a relevant geometrical parameter that should be taken into consideration. All the reported calculations for the transition structure corresponding to the 4π conrotatory ring closure of butadiene have shown a prominent nonplanarity of its carbon skeleton; the calculated dihedral angle ω has a value of 22° at the MP2/6-31G* level.[36] This nonplanarity provides the optimal interaction between the four orbitals of the molecular skeleton. We have found a similar situation in the formation of the four-membered ring of bicyclic compounds **5** and **7**. The values we calculated for the dihedral angle ω in both transition states **TS2a** and **TS2b** are close to 36°. By comparing the differences in ω values between transition structures **TS2a** and **TS2b** and their intermediates **INTa** and **INTb**, respectively, it is remarkable that the difference between **INTa** and **TS2a** ($\Delta\omega$ = 23.5°) is higher than that found between **INTb** and **TS2b** ($\Delta\omega$ = 16.7°; see Table S1 of the Supporting Information). Therefore, in reaching the second transition state, **INTa** must modify the angle ω to a greater extent than must **INTb**.

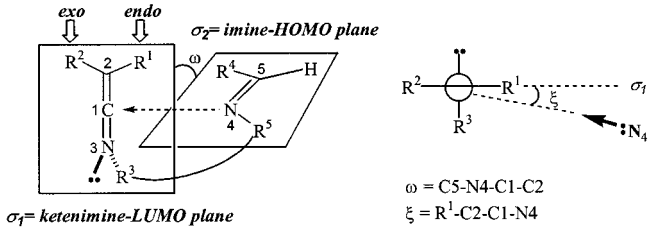

Figure 3. Schematic representation of the interaction between the ketenimine and imine functions showing their LUMO and HOMO planes and some of the dihedral angles that are discussed in the text

The conformational changes that take place along the reaction coordinate on the five-membered ring could affect the energy barrier of this second step. Thus, the *envelope* conformation of the preformed five-membered ring in the dipolar intermediate **INTa** becomes more planar upon reaching the transition structure **TS2a**, which places the C−H bonds in a more-eclipsed disposition and, consequently, this conformation must be higher in energy than that of **INTa**. In contrast, the preformed pyrimidine ring of the zwitterion **INTb** adopts a *sofa* conformation, which does not vary significantly upon approaching the transition state **TS2b**.

Summarizing up to now, this study predicts higher energy barriers for both the first and second reaction steps in the intramolecular cyclization of iminoketenimines **4** leading to **5** relative to those previously reported for the transformation **6** → **7**. Nevertheless, the value of the energy barrier computed for the first step (24.4 kcal mol^{-1}) apparently allows the formation of the intermediate **INTa** under the usual experimental conditions and, since the energy computed for its 4π conrotatory ring closure is only 16.9 kcal mol^{-1}, its forward evolution along the reaction coordinate until the cycloadduct if formed.

With these results in our hands, we still sought an explanation for why the iminoketenimines **1** do not undergo [2+2] cycloaddition, but yield instead the [4+2] cycloadducts. To this goal, we have explored the potential energy surface associated with both types of cycloaddition reactions in the iminoketenimine **8**, a simplified model of **1**, where the vinyl group mimics one of the phenyl groups present in **1**, namely, the one involved in the [4+2] cyclization process (Scheme 5). In Scheme 6 we show the three different reaction paths that we have explored for the transformation of the iminoketenimine **8**: one leading to the [4+2] cycloadduct **10** and two others connecting it with the [2+2] product **9**. The computed energy barriers are listed in Table 2, and the qualitative reaction profiles for the transformations **8** → **9** and **8** → **10** are illustrated in Figure 4. The principal geometrical features of the stationary points are represented in Figure 5.

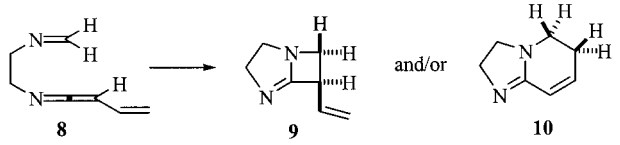

Scheme 5

Table 2. Energy barriers (ΔE, kcal mol^{-1}) computed for the transformations **8** → **9** and **8** → **10**

	ΔE_1[a]	ΔE_2	ΔE_3	ΔE^9_{rxn}[b]	ΔE^{10}_{rxn}		
Method	*endo*	*exo*	*endo*	*exo*			
HF/6-31G*[c]	36.02	32.98	27.94	26.85	15.55	−8.13	−45.65
B3LYP/6-31G*[d]	22.77	20.77	16.31	14.37	6.38	−6.28	−42.00
MP2/6-31G*[e]	22.12	20.49	12.15	10.75	7.72	−14.71	−50.80

[a] See Figure 4 for the notation of the energy barriers. [b] Energy barrier computed for the transformation of **8** into the most stable [2+2] cycloadduct, *endo*-**9**. [c] Energies computed on fully optimized HF/6-31G* geometries. The ZPVE corrections computed at the same level and appropriately scaled have been included. [d] Energies computed on fully optimized B3LYP/6-31G* geometries. The ZPVE corrections computed at the same level have been included. [e] Energies computed on fully optimized MP2/6-31G* geometries. The ZPVE corrections computed at the same level and appropriately scaled have been included.

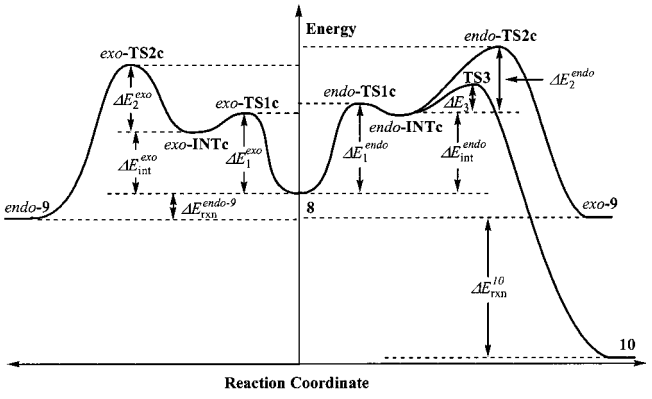

Figure 4. Qualitative reaction profiles of the intramolecular [2+2] and [4+2] cycloadditions of **8** to yield the cycloadducts **9** and **10**, respectively, computed at the B3LYP/6-31G* level of theory

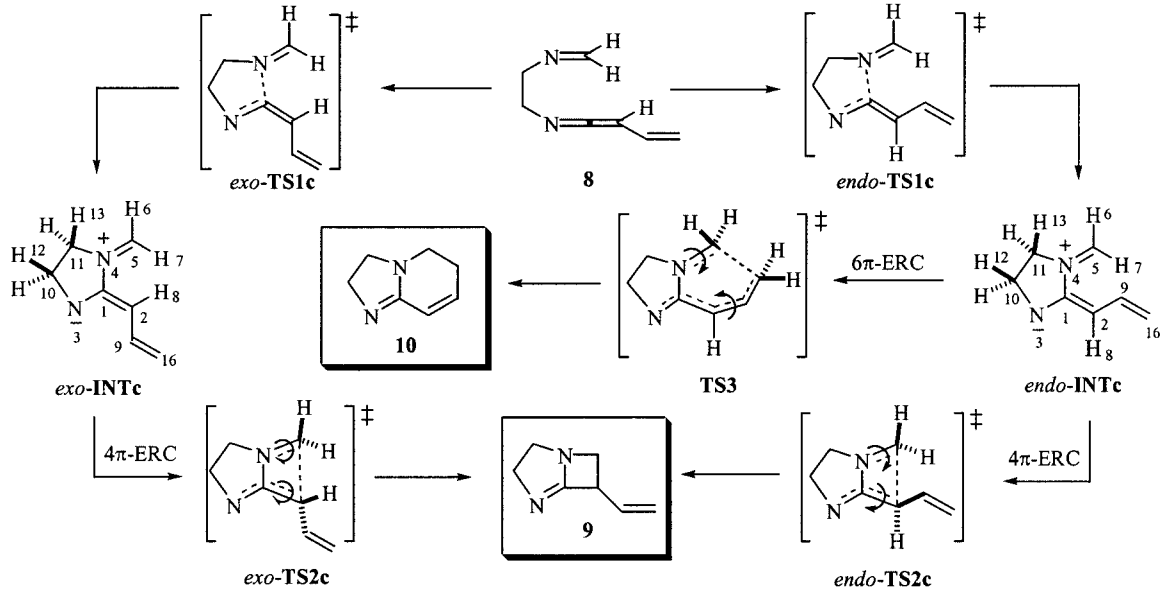

Scheme 6

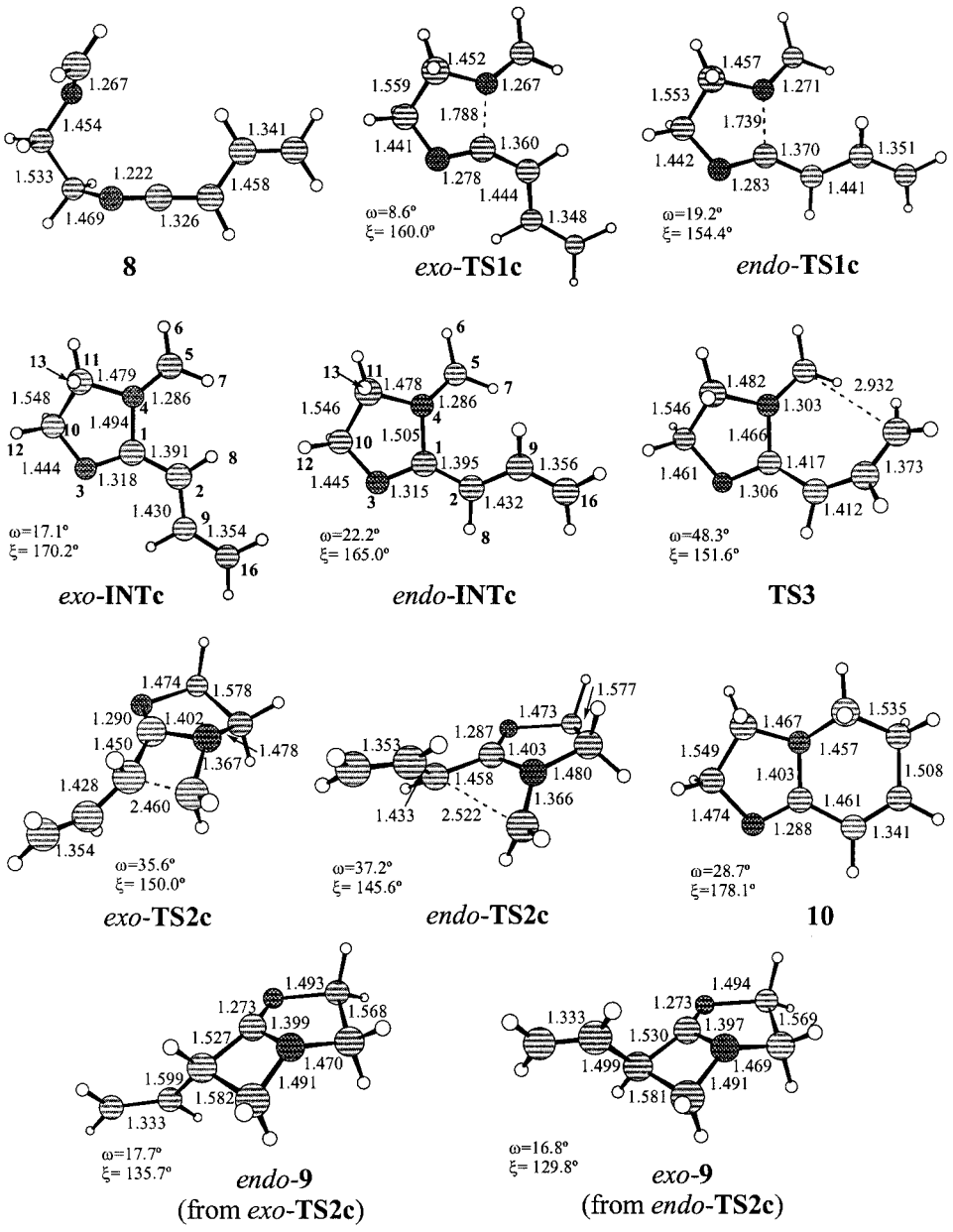

Figure 5. Computer plot of the stationary points found in the intramolecular [2+2] and [4+2] cycloadditions of **8** to yield **9** and **10**, respectively; plain numbers correspond to the geometrical parameters computed at the B3LYP/6-31G* level

An intensive search along the potential energy surface of **8** revealed a series of stepwise mechanisms and, once again, all attempts to find concerted reaction pathways were unsuccessful. Most interestingly, this search allowed us to establish that *both the [2+2] and [4+2] cycloadducts* ***9*** *and* ***10*** *are formed from common zwitterionic intermediates.*

Because the ketenimine function of **8** is monosubstituted at its terminal carbon atom, the nucleophilic attack of the iminic nitrogen atom can take place by two alternative paths, depending on the *endo* or *exo* positioning of the vinyl group with regard to the forming C−N bond. Consequently, two diastereoisomeric transition states were located: namely, *exo*-**TS1c** and *endo*-**TS1c**.

The transition structure *exo*-**TS1c** is earlier than *endo*-**TS1c**; the latter exhibits a shorter N4−C1 bond length (1.788 vs. 1.739Å). The optimal angle[11] of attack of the iminic nitrogen atom to the LUMO plane of the ketenimine moiety, ξ (R1−C2−C1−N4), is 0° (see Figure 3). This torsional angle ξ is slightly greater in *endo*-**TS1c** (32 vs. 24°; see Table S2 of Supporting Information), which indicates a higher departure from the most favorable trajectory during the cyclization step leading to *endo*-**INTc**, the transition state of which is only 2 kcal mol^{-1} higher in energy than its *exo* counterpart.

Following on from both these transition structures, the respective zwitterionic intermediates, *endo*-**INTc** and *exo*-

INTc, are formed, the most stable, by 3.1 kcal mol^{-1}, being *exo*-**INTc**. This relative stability probably is due to the more-congested steric environment of the *endo* zwitterion nearby the methylene proton H7. This situation is also apparent when analyzing some of the geometrical parameters of both intermediates, such as the value of the ω torsional angle, which is greater in *endo*-**INTc** (22°) than in *exo*-**INTc** (17°), and the length of the C1−N4 bond, which is slightly shorter in *exo*-**INTc**. By comparison with the analogous polar intermediate **INTa** that we analyzed above, it is noteworthy that the C1−C2 and C5−N4 bonds are larger, and the C1−N4 bond shorter, for both *endo*- and *exo*-**INTc**; these phenomena are due, most probably, to the conjugation of the vinyl group with the azabutadiene moiety, C2=C1−N4=C5. This hypothesis is also supported by the difference in natural charges between C2 and C5 in **INTa** [$\Delta\Sigma q$ (C^2-C^5) = 0.71] being higher than those in *endo*- and *exo*-**INTc** (0.58 and 0.62, respectively; see Table S2 of Supporting Information).

Two transition structures, *endo*- and *exo*-**TS2c**, are associated with the C2−C5 bond formation; they correspond to the conrotatory ring closures of *endo*- and *exo*-**INTc**, respectively, both of which lead to the cycloadduct **9**. Because of the pyramidalization of the bridgehead nitrogen atom (N4) of the bicyclic compound **9**, two diastereoisomeric [2+2] cycloadducts, namely *exo*-**9** and *endo*-**9**, are formed, one from each diastereoisomeric transition structure, *endo*-**TS2c** and *exo*-**TS2c**, respectively (Figure 5). Note that in **9**, the *endo* and *exo* prefixes now indicate the positioning of the vinyl group toward the concave and convex sides of the molecule, respectively. Bicyclic compound *endo*-**9** is slightly lower in energy (only 0.7 kcal mol^{-1}) than *exo*-**9**. Both diastereoisomeric [2+2] cycloadducts are interconverted by inversion of the bridgehead nitrogen atom (N4), with concomitant ring inversion, at a very low energetic cost (4.92 kcal mol^{-1} for the conversion of *endo*-**9** into *exo*-**9**).

The vinyl group in the intermediate *exo*-**INTc** is in an *outward*[37] disposition with respect to the future C2−C5 bond, which will be formed through *exo*-**TS2c**. In contrast, the vinylic fragment in *endo*-**INTc** is placed *inward*. According to the torquoelectronic theory,[38] the relative energies of both transition structures, *endo*-**TS2c** and *exo*-**TS2c**, will depend mainly on the *inward* or *outward* disposition of the

$$\mathbf{8} \underset{k_{-1}^{endo}}{\overset{k_1^{endo}}{\rightleftharpoons}} \textit{endo}\text{-}\mathbf{INTc} \overset{k_2^{endo}}{\nearrow} \textit{exo}\text{-}\mathbf{9} \quad \textit{endo}\text{-}\mathbf{INTc} \overset{k_3}{\searrow} \mathbf{10} \tag{1}$$

$$\mathbf{8} \underset{k_{-1}^{exo}}{\overset{k_1^{exo}}{\rightleftharpoons}} \textit{exo}\text{-}\mathbf{INTc} \xrightarrow{k_2^{exo}} \textit{endo}\text{-}\mathbf{9} \tag{2}$$

$$\frac{d\,[\textit{endo}\text{-}\mathbf{INTc}]}{dt} = k_1^{endo}[\mathbf{8}] - (k_{-1}^{endo} + k_2^{endo} + k_3)[\textit{endo}\text{-}\mathbf{INTc}] = 0 \tag{3}$$

$$\frac{d\,[\textit{exo}\text{-}\mathbf{INTc}]}{dt} = k_1^{exo}[\mathbf{8}] - (k_{-1}^{exo} + k_2^{exo})[\textit{exo}\text{-}\mathbf{INTc}] = 0 \tag{4}$$

$$\frac{[\mathbf{9}\ (\text{via } \textit{exo}\text{-}\mathbf{INTc})]}{[\mathbf{10}]} = \frac{k_2^{exo}[\textit{exo}\text{-}\mathbf{INTc}]}{k_3\,[\textit{endo}\text{-}\mathbf{INTc}]} = \frac{k_2^{exo} k_1^{exo} (k_{-1}^{endo} + k_2^{endo} + k_3)}{k_3\, k_1^{endo} (k_{-1}^{exo} + k_2^{exo})} =$$

$$= \frac{\exp[-(\Delta E_2^{exo} + \Delta E_1^{exo})/\mathrm{RT}][\exp(-\Delta E_{-1}^{endo}/\mathrm{RT}) + \exp(-\Delta E_2^{endo}/\mathrm{RT}) + \exp(-\Delta E_3/\mathrm{RT})]}{\exp[-(\Delta E_3 + \Delta E_1^{endo})/\mathrm{RT}][\exp(-\Delta E_{-1}^{exo}/\mathrm{RT}) + \exp(-\Delta E_2^{exo}/\mathrm{RT})]} \tag{5}$$

$$\frac{[\mathbf{9}\ (\text{via } \textit{endo}\text{-}\mathbf{INTd})]}{[\mathbf{10}]} = \frac{k_2^{endo}[\textit{endo}\text{-}\mathbf{INTc}]}{k_3\,[\textit{endo}\text{-}\mathbf{INTc}]} = \frac{k_2^{endo}}{k_3} = \exp[-(\Delta E_2^{endo} - \Delta E_3)/\mathrm{RT}] \tag{6}$$

$$\Delta E_{-1}^{endo} = \Delta E_1^{endo} - \Delta E_{int}^{endo} \tag{7}$$

$$\Delta E_{-1}^{exo} = \Delta E_1^{exo} - \Delta E_{int}^{exo} \tag{8}$$

$$k = \frac{K_B T}{h}[\exp-(\Delta E/\mathrm{RT})] \tag{9}$$

vinyl group, which is considered to be a weak donor substituent ($\sigma_R^\circ = -0.03$).[39] Therefore, the conrotatory mode with the vinyl group *inward* is destabilized relative to the *outward* positioning, which accounts for the higher stability of *exo*-**TS2c** relative to *endo*-**TS2c** (5.06 kcal mol^{-1}). Houk et al. studied the effects of the substituents on the rates and stereoselectivities of the conrotatory ring opening of cyclobutenes,[40] computing a difference of 4.9 kcal mol^{-1} (MP2/6-31G*//HF-3−21G level) between the energy barriers of the *inward* and *outward* conrotations of 3-vinylcyclobutene; this value is very close to the one computed here at the B3LYP/6-31G* level for the energy difference between *exo*- and *endo*-**TS2c**.

Alternatively, the polar intermediate *endo*-**INTc** is connected to the [4+2] cycloadduct by a second route, namely a disrotatory 6π ring closure occurring via the saddle point **TS3**. The energetic cost for this pathway is considerably lower than the one associated with its conrotatory 4π ring closure leading to **9**, since **TS3** is 9.94 kcal mol^{-1} lower in energy than *endo*-**TS2c**. The total enthalpy associated with the formation of the [4+2] cycloadduct is −42.0 kcal mol^{-1}, while that corresponding to the formation of **9** is −6.3 kcal mol^{-1}. Accordingly, the [4+2] cycloadduct **10** is the product of both kinetic and thermodynamic control in the cyclization of zwitterionic *endo*-**INTc**.

We have calculated the relative ratio of products **9** and **10** that this theoretical treatment predicts by performing a quantitative kinetic analysis that considers the system represented by Equations (1) and (2). From the computational results, we can assume that [*exo*-**INTc**] << [**9**] and [*endo*-**INTc**] << [**9**] + [**10**], and, consequently, the steady-state approximation[41] can be applied [Equations (3) and (4) yielding Equations (5) and (6)].

From Equations (5) and (6) and the data reported in Table 2, we estimated the product selectivity in the transformation **8** → **9** and/or **10**. Thus, at 298 K, we calculated values of 5.26×10^{-8}:2.65×10^{-4}:1 for the ratio of **9** (via *endo*-**INTc**) to **9** (via *exo*-**INTc**) to **10**; i.e., 99.97% of the [4+2] cycloadduct **10** versus 0.03% of the [2+2] cycloadduct **9**. It is remarkable that product **9** is predicted to be formed exclusively via *exo*-**INTc**, but not via *endo*-**INTc**. This finding is due to the higher energetic cost for reaching *endo*-**TS1c** relative to that of *exo*-**TS1c** and because intermediate *endo*-**INTc** only transforms into the [4+2] cycloadduct **10** since $\Delta E_2(endo) >> \Delta E_3$.

Iminoketenimines **1**, which were utilized in the experimental study, should lead to a unique zwitterionic intermediate since the *exo* and *endo* modes of attack are equivalent because both substituents on the terminal carbon atom of the ketenimine moiety are identical (two phenyl groups). The predicted ratio of final products can be calculated from the expression [2+2]/[4+2] = k_2/k_3, and, therefore, will depend only on the difference between the values ΔE_2 and ΔE_3. Consequently, our theoretical approach predicts that the iminoketenimines **1** should yield exclusively the corresponding [4+2] cycloadducts; the formation of the [2+2] cycloadducts should be negligible.

It can be argued, not without sense, that a vinyl group is not a good model of a phenyl unit, especially in the 6π ring closure step leading to the [4+2] cycloadduct, where it cannot account for the loss of aromaticity that follows the participation of a C=C bond belonging to a real phenyl group. For a more reliable approach, we optimized, at the B3LYP/6-31G* level of theory, the zwitterion **INTd**, arising from *C*-phenyl iminoketenimine **11**, and located the transition structures **TS2d** and **TS3d** corresponding to its two cyclization modes, 4π and 6π-electrocyclic ring closures, that lead to the corresponding [2+2] and [4+2] cycloadducts, respectively (Scheme 7).

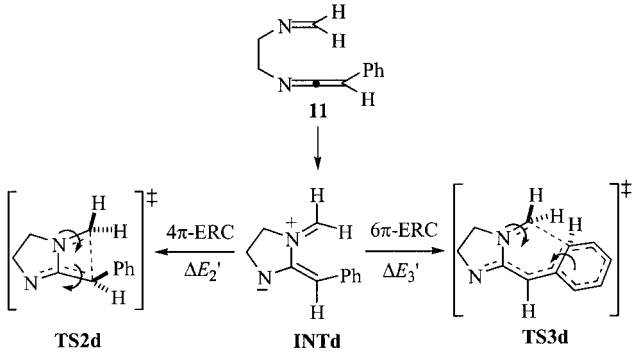

Scheme 7

As presumed, the calculated energy barrier ($\Delta E_{3'}$) for the 6π electrocyclization of **INTd** is higher than that previously obtained for its vinyl analogue *endo*-**INTc** (12.53 vs. 6.38 kcal mol^{-1}); what is more relevant, however, is that $\Delta E_{3'}$ is still 3.6 kcal mol^{-1} lower than the energy barrier ($\Delta E_{2'}$) of the 4π electrocyclization of **INTd**, despite the preservation of the aromaticity of the phenyl group in this last step. By translating these data to the kinetic equations, a product selectivity of 99.8:0.2 is predicted in favor of the [4+2] cycloadduct.

In summary, this computational study explains satisfactorily the experimental outcomes obtained previously, especially the preference of the iminoketenimines **1** to undergo [4+2] cycloaddition reactions exclusively instead of their alternative [2+2] modes.

Conclusion

The present computational calculations have established the mechanism of the intramolecular cyclization of *N*-(iminoethylene) ketenimines into their corresponding [2+2] cycloadducts. The reaction path is stepwise and involves a zwitterionic intermediate. The mechanism and the mode-selective course of the intramolecular cyclizations of *C*-phenyl-substituted iminoketenimines, which lead exclusively to the corresponding [4+2] cycloadducts, have been rationalized. Both the [2+2] and [4+2] cycloadducts are formed from common polar intermediates, and the energetic cost for the 4π electrocyclic ring closure of the zwitterion yielding the [2+2] cycloaddition product is higher than that of

its 6π disrotatory ring closure leading to the [4+2] cycloadduct. The quantitative kinetic analysis for estimating the relative ratio of cyclization products provides a good agreement with the experimental results.

Supporting Information: Tables S1−S4, including the chief geometric and energetic features, first frequencies, and natural charges of all stationary points discussed in the text; Cartesian coordinates of local minima and transition structures discussed in the text (see also footnote on the first page of this article).

Acknowledgments

This work was supported by the MCYT and FEDER (Project BQU2001−0010), Fundación Seneca-CARM (Project PI-1/00749/FS/01), and Acedesa (a division of Takasago). We are also grateful to Prof. F. P. Cossío for useful comments. P. S.-A. warmly thanks the Universidad de Murcia for a fellowship.

[1] M. W. Barker, W. E. McHenry, *Chemistry of Ketenes, Allenes, and Related Compounds* (Ed.: S. Patai), Wiley-Interscience, Chichester, UK, **1980**, Part 2, pp. 701−720.
[2] G. R. Krow, *Angew. Chem. Int. Ed. Engl.* **1971**, *10*, 435−449.
[3] M. Alajarín, A. Vidal, F. Tovar, *Targets Heterocycl. Syst.* **2000**, *4*, 293−326, and references cited therein.
[4] A. Dondoni, *Heterocycles* **1980**, *14*, 1547−1566.
[5] N. P. Gambaryan, *Usp. Khim.* **1976**, *45*, 1251−1268.
[6] M. A. Walters, *J. Am. Chem. Soc.* **1994**, *116*, 11618−11619, and references cited therein.
[7] B. Arnold, M. Regitz, *Angew. Chem. Int. Ed. Engl.* **1979**, *18*, 320.
[8] A. Van Camp, D. Goossens, M. Moya-Portugez, J. Marchand-Brynaert, L. Ghosez, *Tetrahedron Lett.* **1980**, *21*, 3081−3084.
[9] M. Alajarín, P. Molina, A. Vidal, *Tetrahedron Lett.* **1996**, *37*, 8945−8948.
[10] M. Alajarín, P. Molina, A. Vidal, F. Tovar, *Tetrahedron* **1997**, *53*, 13449−13472.
[11] M. Alajarín, A. Vidal, F. Tovar, A. Arrieta, B. Lecea, F. P. Cossío, *Chem. Eur. J.* **1999**, *5*, 1106−1117.
[12] F. P. Cossío, A. Arrieta, B. Lecea, M. Alajarín, A. Vidal, F. Tovar, *J. Org. Chem.* **2000**, *65*, 3633−3643.
[13] M. Alajarín, A. Vidal, F. Tovar, F. P. Cossío, A. Arrieta, B. Lecea, *J. Org. Chem.* **2000**, *65*, 7512−7515.
[14] M. Alajarín, A. Vidal, R.-A. Orenes, *Eur. J. Org. Chem.* **2002**, 4222−4227.
[15] G. Barbaro, A. Battaglia, P. Giorgianni, *J. Org. Chem.* **1987**, *52*, 3289−3296.
[16] M. Alajarín, A. Vidal, F. Tovar, C. Conesa, *Tetrahedron Lett.* **1999**, *40*, 6127−6130.
[17] M. Alajarín, A. Vidal, F. Tovar, *Tetrahedron Lett.* **2000**, *41*, 7029−7032.
[18] M. Alajarín, A. Vidal, F. Tovar, P. Sánchez-Andrada, D. Bautista, *Tetrahedron* **2003**, *59*, 9913−9918.
[19] M. Alajarín, A. Vidal, F. Tovar, P. Sánchez-Andrada, *Tetrahedron Lett.* **2002**, *43*, 6259−6261.
[20] For a related DFT study on the mode selectivity ([2+2] vs. [4+2] cycloaddition) of the reactions of conjugated ketenes with imines, see: C. Zhou, D. M. Birney, *J. Am. Chem. Soc.* **2002**, *124*, 5231−5241.
[21] M. J. Frisch, G. W. Trucks, H. B. Schlegel, G. E. Scuseria, M. A. Robb, J. R. Cheeseman, V. G. Zakrzewski, J. A. Montgomery, Jr., R. E. Stratmann, J. C. Burant, S. Dapprich, J. M. Millam, A. D. Daniels, K. N. Kudin, M. C. Strain, O. Farkas, J. Tomasi, V. Barone, M. Cossi, R. Cammi, B. Mennucci, C. Pomelli, C. Adamo, S. Clifford, J. Ochterski, G. A. Petersson, P. Y. Ayala, Q. Cui, K. Morokuma, D. K. Malick, A. D. Rabuck, K. Raghavachari, J. B. Foresman, J. Cioslowski, J. V. Ortiz, A. G. Baboul, B. B. Stefanov, G. Liu, A. Liashenko, P. Piskorz, I. Komaromi, R. Gomperts, R. L. Martin, D. J. Fox, T. Keith, M. A. Al-Laham, C. Y. Peng, A. Nanayakkara, M. Challacombe, P. M. W. Gill, B. Johnson, W. Chen, M. W. Wong, J. L. Andres, C. Gonzalez, M. Head-Gordon, E. S. Replogle, J. A. Pople, *Gaussian 98, Revision A.9*, Gaussian, Inc., Pittsburgh PA, **1998**.
[22] R. G. Parr, W. Yang, *Density-Functional Theory of Atoms and Molecules*, Oxford University Press, New York, **1989**.
[23] L. J. Bartolotti, K. Fluchichk, *Reviews in Computational Chemistry* (Eds.: K. B. Lipkowitz, D. B. Boyds), VCH Publishers, New York, **1996**, vol. 7, pp. 187−216.
[24] W. Kohn, A. D. Becke, R. G. Parr, *J. Phys. Chem.* **1996**, *100*, 12974−12980.
[25] T. Ziegler, *Chem. Rev.* **1991**, *91*, 651−667.
[26] C. Moller, M. S. Pleset, *Phys. Rev.* **1934**, *46*, 618−622.
[27] M. J. Frisch, M. Head-Gordon, J. A. Pople, *Chem. Phys. Lett.* **1990**, *166*, 281−289.
[28] M. J. Frisch, M. Head-Gordon, J. A. Pople, *Chem. Phys. Lett.* **1990**, *166*, 275−280.
[29] J. S. Binkley, J. A. Pople, *Int. J. Quantum Chem.* **1975**, *9*, 229−236.
[30] J. A. Pople, J. S. Binkley, R. Seeger, *Int. J. Quantum Chem. Symp.* **1976**, *10*, 1−19.
[31] W. J. Hehre, L. Radom, P. v. R. Schleyer, J. A. Pople, *Ab Initio Molecular Orbital Theory*, Wiley, New York, **1986**, pp. 71-82, and references cited therein.
[32] J. A. Pople, H. B. Schlegel, R. Krishnan, D. J. DeFrees, J. S. Binkley, M. J. Frisch, R. A. Whiteside, R. F. Hout Jr., W. J. Hehre, *Int. J. Quantum Chem. Symp.* **1981**, *15*, 269−278.
[33] A. E. Reed, R. B. Weinstock, F. Weinhold, *J. Chem. Phys.* **1985**, *83*, 735−746.
[34] A. E. Reed, L. A. Curtiss, F. Weinhold, *Chem. Rev.* **1988**, *88*, 899−926.
[35] A. E. Reed, P. v. R. Schleyer, *J. Am. Chem. Soc.* **1990**, *112*, 1434−1445.
[36] D. C. Spellmeyer, K. N. Houk, *J. Am. Chem. Soc.* **1988**, *110*, 3412−3416.
[37] K. Rudolf, D. C. Spellmeyer, K. N. Houk, *J. Org. Chem.* **1987**, *52*, 3708−3710, and references cited therein.
[38] W. R. Dolbier Jr., H. Koroniak, K. N. Houk, C. Sheu, *Acc. Chem. Res.* **1996**, *29*, 471−477.
[39] N. S. Isaacs, *Physical Organic Chemistry*, Longman, Essex, **1987**, p. 158, and references cited therein.
[40] S. Niwayama, E. A. Kallel, D. C. Spellmeyer, C. Sheu, K. N. Houk, *J. Org. Chem.* **1996**, *61*, 2813−2825.
[41] J. H. Espenson, *Chemical Kinetics and Reaction Mechanisms*, McGraw-Hill, New York, **1981**, pp. 72, 87.

Received February 11, 2004

